Invited Paper

Thermal emission from metallic films perforated with subwavelength hole arrays

Mohit Diwekar[a], Tatsunosuke Matsui*[a], Amit Agrawal[b], Ajay Nahata[b], Z. Valy Vardeny+[a]
[a] Department of Physics, University of Utah, Salt Lake City, UT USA 84112;
[b] Department. of Electrical and Computer Engineering, University of Utah, Salt Lake City, UT USA 84112

ABSTRACT

This report presents an overview of our study on the optical transmission and thermal light emission properties of sub-wavelength hole arrays fabricated in a square lattice with 4 μm periodicity. The structures were fabricated in thin aluminum (Al) films on silicon (Si) substrates using conventional photolithography. The spectra were obtained using a Fourier transform infrared spectrometer with a port for an external cryostat configured for thermal emission measurements. The perforated films showed extraordinary transmission bands in the mid-infrared spectral range, which could be well explained as due to light coupling to surface plasmon-polaritons on the two film interfaces. We fitted the transmission spectra and calculated the absorption spectra of these structures using a model for the dielectric response that utilizes an effective plasma frequency determined by the individual holes, as well as several resonant modes associated with the reciprocal vectors in the lattice structure factor. We found that the thermal emission spectrum from the perforated films followed the transmission spectrum characteristics, rather than the obtained absorption spectrum; in apparent contrast to Kirchhoff's law of radiation. We conclude that the perforated films behave as *radiation filters*, where the thermal emission radiation is suppressed in the frequency range outside the transmission resonant bands in the spectrum.

Keywords: Photonic Crystals, Metallic Hole arrays, Thermal emission, Mid-Infrared optical transmission

1. INTRODUCTION

Collective excitations of the electronic density on a surface of smooth metallic film lead to surface plasmon polaritons (SPP). Light is does not couple to SPP on such films, because conservation of energy, E and momentum, $\mathbf{k}$ cannot be obeyed simultaneously [1]. On a (E, $\mathbf{k}$) plot, the SPP dispersion curve lies below that of electromagnetic waves in vacuum. Also metallic films whose thickness is greater than the optical skin depth are opaque to light at frequencies below the bulk plasma frequency. However, in a metallic film that is perforated with two-dimensional (2D) periodic array of holes that forms a 2D metallo-dielectric photonic crystal, the periodicity allows for grating coupling of the SPP light to lightSPP, which results in resonantly enhanced transmission bands, also referred to as 'anomalous transmission' or 'extraordinary optical transmission' (EOT). The EOT phenomenon was discovered approximately a decade ago in groundbreaking work by Ebbesen *et al.* where the optical transmission through a perforated Al film in the visible/near-infrared spectral range was measured [2]. This work launched a large number of experimental and theoretical studies on perforated metal films with subwavelength hole arrays or 'plasmonic lattices' having both periodic [2-20], aperiodic [21-25], and even fractal [26] structures. The intense interest in the EOT phenomenon is partially due to potential wide-ranging applications in near-field microscopy [27], optoelectronics [28, 29], and biosensing [30]. Most of the experimental work to date has dealt with EOT in the visible, near-infrared and THz spectral ranges. It has been recognized [15, 23] that the resonant transmission bands have different properties in these two spectral ranges, since the SPP attenuation is much larger in the visible spectral range. However, relatively few EOT studies have been performed in the mid-infrared (MIR) spectral range [16, 31]. The MIR range is particularly interesting since the SPP attenuation is still low in this range; and in addition commonly available MIR spectrometers may be used without the necessity of sophisticated experimental tools such as those needed in the THz range.

* Present address: Department of Electrical and Computer Engineering, Mie University, 1577 Kurimamachiya, Tsu, Mie 514-8507, Japan

+ val@physics.utah.edu; phone 1 801 581-8372; fax 1 801 581-4801

Plasmonics: Nanoimaging, Nanofabrication, and Their Applications IV, edited by Satoshi Kawata, Vladimir M. Shalaev, Din Ping Tsai, Proc. of SPIE Vol. 7033, 70331E, (2008) · 0277-786X/08/$18 · doi: 10.1117/12.796091

Approximately at the same time of the discovery of EOT through plasmonic lattices, it was suggested that thermal emission radiation from a metallic array should be very different from the well-known Planck blackbody emission spectrum [32]. Specifically the calculated emission spectrum was found to be strongly affected by resonances in the optical spectra. This work has initiated a number of investigations aimed at studying the modification of the thermal emission spectrum from 3D metallic photonic crystals [33-42], where strong changes in the emission spectrum compared to metals have been observed. Also a controversy was recently noticed, where the claim that the thermal emission efficiency of 3D metallic photonic crystals is larger than that of a blackbody was challenged [40, 41]. So far most of the studies of thermal emission from photonic structures have been performed using 3D photonic crystals [32-42]. However 2D photonic crystals might also change the photonic density of states (DOS) of the heated metals and consequently alter the thermal emission spectrum. In particular, it is not clear whether perforated metallic films in the form of a 2D plasmonic lattice that show EOT are sufficiently strong photonic crystals that their thermal emission spectrum can be modified.

In this work, we report our studies of the optical transmission and thermal emission spectra from subwavelength hole arrays fabricated in square lattice symmetry with 4 μm periodicity in aluminum (Al) thin films. We found the existence of EOT resonances and anti-resonances (AR) in the MIR spectral range, which can be well explained by light coupling to SPP excitations. From the EOT spectrum, we calculated the effective dielectric function and the corresponding absorption spectrum of the perforated metal films using a recently suggested model. In this model, the individual holes determine the effective plasma frequency, whereas the reciprocal vectors in the lattice structure factor determine the resonant modes. We found that the absorption spectrum of the perforated film exhibits an inverse optical modulation of the transmission spectrum; namely absorption peaks (dips) replace transmission dips (peaks) in the spectrum. We also found that the thermal emission from the perforated film is modified compared to that of an un-patterned film. Although the obtained changes in the emissivity spectrum are small, the overall thermal emission spectrum is still strongly altered, primarily because the hole array structure acts as a *radiation filter*, where the emission is suppressed outside of the resonant EOT bands. This optical filtering is characteristic of *weak* photonic crystals, where the photon DOS in the heated metal film is weakly modified by the perforated interfaces, suggesting weak coupling between the SPP excitations on the metal/dielectric interfaces and the MIR photonic states inside the metal film.

2. EXPERIMENTAL

Al films were deposited on Si substrates using an e-beam evaporator with a thickness of about 300 nm. The hole array structure with square lattice symmetry were then fabricated using standard photolithographic processes. After patterning the photo-resist, the periodic hole array pattern was transferred onto the underlying metal films by a reactive ion-etching method. The fabricated hole array lattice constant was 4 μm with hole diameter of 2.46 μm (Fig. 1 inset). To characterize the spectral response of these metallo-dielectric arrays we used a Fourier Transform infrared (FTIR) spectrometer. The optical transmission spectrum, $T(\omega)$ in the MIR spectral range was measured through the hole arrays at normal incidence and then was normalized by the transmission spectrum of a bare Si substrate in the same spectral range. The Al film is opaque in the MIR spectral range, and thus the obtained anomalous transmission bands are due to the individual holes in relation with interference resonances from light coupling to SPP on the two Al film interfaces [2].

The experimental setup for measuring the thermal emission spectra from the heated metallic films was properly configured to minimizing background emission that might interfere with the main thermal emission spectrum from the sample (Fig. 2). This was achieved by mounting the samples in a liquid nitrogen cooled vacuum chamber that was pumped down to approximately 10^{-5} Torr. The sample was mounted on a NiCr wire heating coil and subsequently heated to a temperature $T \sim 600$K. The thermal emission radiation passed through a KBr cryostat window, and was fed into an external port of the FTIR spectrometer for spectral analysis. A KBr beam-splitter and a DTGS-MIR photodetector were used for the MIR signal detection. This photodetector/beam-splitter combination has a fairly flat spectral response in the MIR spectral range from 4 to 20 μm.

3. RESULTS AND DISCUSSION

3.1 Extraordinary transmission spectra

As seen in Fig. 1 the transmission spectrum, T(ω) from the fabricated perforated metallic films contains a broad enhanced transmission band starting from ~ 400 cm^{-1}, as well as several resonant transmission bands (indexed 1 to 5), each followed by a respective anti-resonance dip on the high frequency side that are due to the hole array lattice periodicity [2, 11]. Similar EOT features have been obtained previously in T(ω) in the visible [2] and THz [11, 23] spectral ranges through perforated metal structures with appropriate lattice constants that match the resonant wavelengths. These EOT resonances have been explained by a model that involves SPP coupling to light on the perforated metal surfaces [2]. A modification of this model [43] is described below.

An incident light that impinges on a smooth metallic surface at normal angle cannot excite SPP excitations, as these excitations can exist only in the transverse magnetic mode on such a metallic surface [1]. However the periodically spaced holes on the metallic surface allow for grating-coupling between the incident light and SPP excitations on the two film interfaces. The conservation of quasi-momentum in this case is usually written as [2],

$$\vec{k}_{sp} = \vec{k}_x \pm m\vec{u}_x \pm n\vec{u}_y \tag{1}$$

where $\left|\vec{k}_x\right| = (\frac{2\pi}{\lambda})\sin\theta$ is the component of the incident light wave-vector in the plane of the hole array, and $\vec{u}_x$ and $\vec{u}_y$ are the primitive reciprocal lattice vectors. For a square lattice we have $\left|\vec{u}_x\right| = \left|\vec{u}_y\right| = \left(\frac{2\pi}{a_0}\right)$; where a_0 is the lattice constant of the hole array structure, and m, n are integers. From the conservation of energy we get for the SPP wave-vector, k_{spp} on a smooth metallic film

$$\left|\vec{k}_{spp}\right| = \frac{\omega}{c}\left(\frac{\varepsilon_m(\omega)\varepsilon_d}{\varepsilon_m(\omega)+\varepsilon_d}\right)^{\frac{1}{2}} \tag{2}$$

where $\varepsilon_m(\omega)$ and ε_d are the respective dielectric constants of the metal film and substrates; Si or air. At normal incidence and for $\varepsilon_m >> \varepsilon_d$, Eqs. (1) and (2) can be reduced for obtaining the wavelengths, λ_{min} of the AR's features in T(ω) spectrum, as following:

$$\lambda_{MIN} = \frac{a_0}{\sqrt{m^2+n^2}}\sqrt{\varepsilon_d} \tag{3}$$

The AR in T(ω) can then be assigned to SPP modes with specific n, m integer parameters associated with the two interfaces, as seen in Fig. 1. The four AR modes (or Wood's anomalies [2, 11]) for the Al/Si interface, and the single mode for the Al/air interface are summarized in Table I, and compared with the theoretical values based on Eq. (3), where ε_d for Si was taken from known literature tables. The agreement between the experimental and theoretical λ_{min} values is remarkable, showing that the SPP model works very well in the MIR range, *but for the AR frequencies* rather than the resonant peaks in T(ω); this is in contrast to the EOT bands in the visible range, where the SPP attenuation has to be taken into account. Nevertheless we believe that in order to assign the resonant EOT peaks in T(ω), and get further insight into the nature of the SPP excitations on a perforated metallic film, one must use the '*actual*' form of $\varepsilon_m(\omega)$, as opposed to using the metallic dielectric function from a standard database of an un-patterned bulk metal.

We recently proposed to determine the 'effective' dielectric constant, $\varepsilon_m(\omega)$ for perforated metallic films using an 'effective plasma frequency' model [43] and adopt this model here. The dielectric function $\varepsilon_m(\omega)$ used in our calculation was in the following form:

$$\varepsilon_m(\omega) = \varepsilon_\infty \left[1 - \left(\frac{\tilde{\omega}_p^{\,2}}{\omega^2 + i\gamma\omega} \right) + \sum_j \left(\frac{\omega_{L_j}^{\,2} - \omega^2}{\omega_{T_j}^{\,2} - \omega^2 - i\gamma_j \omega} \right) \right] \tag{4}$$

where ε_∞ is the high-frequency dielectric constant; $\tilde{\omega}_p$ is the 'effective' plasma frequency related with the *individual* holes; ω_T corresponds to the frequency minima (or AR) in $T(\omega)$; ω_L is an effective 'longitudinal frequency' for the resonant mode that is used here to determine its oscillator strength, S_j (or Rabi frequency) in $\varepsilon_m(\omega)$, given by $S_j = (\omega_L/\omega_T)^2 - 1$; and γ_j corresponds to the respective damping constant. Eq. (4) has both plasmon (first two terms), and resonant modes (third term) characteristics. The effective plasma term comes from the individual, uncorrelated holes in the perforated metal; it does not contain resonances and thus fits the broad band enhanced transmission in $T(\omega)$ that starts at ~ 400 cm^{-1}. In contrast, the 'resonant modes' term in Eq. (4) is related to the structure factor (or periodicity) of the underlying hole arrays [23], where ω_T is the AR frequencies. In the case of zero damping and flat 'plasmon response', the term describing the resonant modes characteristics leads to a modified Lyddane-Sachs-Teller (LST) relation [44]. Eq. (4) is a generalization of the plasma dielectric function (first two terms), and a LST-type dielectric function, $\varepsilon_{LST}(\omega)$ (last term in Eq. (4)), which was used before for describing the optical properties of doped polar semiconductors [45-47]. At temperatures higher than the 'freeze-on impurity' temperature, such a dielectric response contains a plasma term due to the free carriers released by the dopant impurities; in addition to polar phonons with longitudinal optical (LO) and transverse optical (TO) modes that are given by ω_L and ω_T, respectively.

Table 1. The anti-resonant SPP modes in the $T(\omega)$ spectrum associated with the two interfaces of the perforated Al film, namely Al/Si and Al/air. The calculated AR frequencies were obtained using Eq. (3) and ε_d from tables. The uncertainties in the values of the experimental AR frequencies are also given.

Interface	SPP Mode	AR experimental frequencies (cm^{-1})	AR calculated frequencies (cm^{-1})
Al/Si	(1, 0) (1, 1) (2, 0) (2, 2)	756 (±5) 1073 (±15) 1560 (±50) 2150 (±50)	722 1021 1445 2045
Al/air	(1, 0)	2600 (±50)	2500

The optical transmission spectrum was calculated using $\varepsilon_m(\omega)$ from Eq. (4), and fit to the experimental spectrum using a least squares fitting procedure. In the fitting the resonant ω_T were fixed at the AR frequencies, and were taken directly from the experimental $T(\omega)$ spectrum, whereas the plasma parameters $\tilde{\omega}_p$ and γ were fit to the broad continuous transmission band in the spectrum. The other parameters, such as ε_∞, and the respective ω_L and γ for the individual

resonant modes were left free. We focus our attention to the two lower frequency resonant modes, namely (1, 0) and (1, 1) SPP modes associated with the Al/Si interface, that are close to the maximum in the thermal emission spectrum at moderately high metal heating temperature. For purposes of the fitting procedure, we only fit these two resonant modes, while the contribution to $\varepsilon_m(\omega)$ of the other resonant modes at higher frequencies was embedded in the ε_∞ parameter. The calculated $T(\omega)$ spectrum based on the 'best fit' parameters given in Table II is shown in Fig. 3 in comparison with the experimental $T(\omega)$. The good agreement obtained between the two $T(\omega)$ spectra validates the model for $\varepsilon_m(\omega)$ used here. Also the real ($Re[\varepsilon_m(\omega)]$), and imaginary ($Im[\varepsilon_m(\omega)]$) components of the dielectric constant spectra calculated based on the 'best fit' parameters are shown in Fig. 3 inset. It is seen that for each resonant mode $Im[\varepsilon_m(\omega)]$ shows a narrow maximum at a frequency that corresponds to the middle of the resonant feature in $Re[\varepsilon_m(\omega)]$. This response comes from the well-known Kramers-Kronig (KK) relation between the real and imaginary $\varepsilon_m(\omega)$ components, and thus validates our calculation method.

Table 2. The 'best fit' parameters for the calculated $T(\omega)$ spectrum of the Al perforated film (Fig. 3(a)) using the effective dielectric function, $\varepsilon(\omega)$ calculated from Eq. (4) with two resonant modes. The various parameters are defined in Eq.(4) [see text].

ε_∞	$\tilde{\omega}_p$ (Hz)	γ (Hz)	ω_{L1} (Hz)	ω_{L2} (Hz)	γ_1(Hz)	γ_2 (Hz)
3.1	24.6×10^{14}	10.1×10^{14}	12.5×10^{14}	15.4×10^{14}	17.6×10^{12}	39.7×10^{12}

In addition we also calculated the absorption spectrum, $\alpha(\omega)$ of the hole array structure from the obtained dielectric function with the 'best fit parameters' using the expression $\alpha = \omega Im[n(\omega)]/c$; where Im(n) is the imaginary component of the refractive index, and was calculated from the fitted $\varepsilon_m(\omega)$ above, and c is the speed of light. The obtained $\alpha(\omega)$ spectrum is plotted together with $T(\omega)$ in Fig. 3(b). It is apparent that the resonant contribution to $\alpha(\omega)$ are opposite in sign compared with those in $T(\omega)$. The $\alpha(\omega)$ spectrum shows *maxima* at the AR frequencies and *minima* at the resonant frequencies in $T(\omega)$. This is in contrast to the situation in the visible range where it was shown [12] that $\alpha(\omega)$ and $T(\omega)$ shows similar resonant features, where maxima in $\alpha(\omega)$ corresponded with maxima in the EOT spectrum.

3.2 Thermal emission Spectra

In order to eliminate the system spectral response as well as any optical loss during the thermal emission measurements, we computed the hole array normalized emissivity spectrum, $E(\omega)$ from the directly measured emission spectrum, $E_H(\omega)$. $E(\omega)$ was obtained by dividing the hole array emission spectrum by the emission spectrum, $E_M(\omega)$ of an un-patterned metal film having identical thickness and measured at the same heated metal temperature. The procedure we adopted is described below:

$$\begin{aligned} E_H(\omega) &= S(\omega)\xi(\omega)D(\omega) \\ E_M(\omega) &= F(\omega)\xi(\omega)D(\omega) \\ E(\omega) &= \frac{E_H(\omega)}{E_M(\omega)} \end{aligned} \tag{5}$$

In Eq. (5) $\xi(\omega)$ represents the optical propagation loss as thermal emission passes through the spectrometer and reaches the photodetector, and $D(\omega)$ represents the combined optical window and photodetector/beam-splitter spectral response. We note that the Planck distribution function, $K(\omega, T)$ for blackbody radiation emission, which is presumably the same for the heated perforated and un-perforated films at the same temperature, is readily taken into account by this procedure. Consequently it is no longer a factor in the analysis below.

The normalized emissivity spectrum $E(\omega)$ of the Al hole array obtained following the procedure described in Eq. (5) is shown in Fig. 4(a). $E(\omega)$ contains several emission bands, but the modification of the perforated film emissivity spectrum compared to that of an un-perforated film is quite small. This is apparent in Fig. 4(a), where the modification of the emissivity spectrum is seen to be around the value 1. In addition, none of the emissivity bands corresponds to resonances found in the absorption spectrum (Fig 4(b)). In fact, $E(\omega)$ better fits $T(\omega)$ rather than $\alpha(\omega)$ (see Fig. 1). For example, the lowest peak in $E(\omega)$ is observed at about 650 cm^{-1}, close to that of the lowest peak in $T(\omega)$. However this emissivity band is out of phase (opposite) from that in $\alpha(\omega)$, which shows an anti-resonance rather than a peak at ~ 700 cm^{-1}. This is close to the peak in $E(\omega)$ rather than a dip.

In order to ensure that the transmission and absorption spectra are considered at the correct temperature, we measured $T(\omega)$ of the hole array at different sample temperatures (Fig. 5). It is seen that $T(\omega)$ does not change much with the temperature. This validates the conclusion that $E(\omega)$ more closely resembles $T(\omega)$, even when the high sample temperature needed for the radiation emission is taken into account.

From Kirchhoff's law, the emission spectrum of a body (or a surface) in thermal equilibrium is equal to the absorbance, $A(\omega)$ weighted by the blackbody distribution spectrum $K(\omega, T)$ at the temperature T of the measurement, such that [48]

$$E(\omega,T) = A(\omega)K(\omega,T) \tag{6}$$

where $K(\omega, T)$ is given by the expression

$$K(\omega,\mathrm{T}) = \frac{\mathrm{h}\omega^3}{\pi^2 c^3}\left(\frac{\hbar\omega}{e^{\frac{\hbar\omega}{kT}}-1}\right) \tag{7}$$

where h is the Planck constant and k_B is the Boltzmann constant. In Eq. (6) the effect of the photonic DOS of such a complex structure are fully captured through $A(\omega)$. Since $E(\omega)$ does not resemble $\alpha(\omega)$, there appears to be a violation of Kirchhoff's law given in Eq. (6). The apparent violation of Kirchhoff's law may arise from the fact that the response of our system is not in thermodynamic equilibrium [41]. Specifically, there is a temperature gradient across the sample film that is maintained at steady state conditions that is established by the heat flow. However, the fact that $\alpha(\omega)$ differs from $E(\omega)$, while $T(\omega)$ and $E(\omega)$ are closely related suggests that this is not the case here.

We thus conclude from the similarity between the emissivity and transmission spectra that the hole array structure behaves as a *radiation filter*; where the emissivity is suppressed outside the EOT resonant bands. In order to verify this hypothesis we calculated from the measured spectra an effective 'transfer function', $G(\omega)$ using the ratio between the obtained $E(\omega)$ and $\alpha(\omega)$ spectra (see Fig. 6). The close similarity between $G(\omega)$ and $T(\omega)$ measured at the same temperature supports our conclusion. The emissivity spectral characteristics of the hole array is indeed affected compared to an un-perforated film, but primarily through a modification induced by the transmission spectrum. Therefore, we conjecture that in perforated metallic films, there exist *weak coupling* between the MIR photon DOS in the metal and the SPP excitations on the metal interface.

The obtained modified emission $G(\omega)$ and its similarity with $T(\omega)$ that is seen here are analogous to the photoluminescence (PL) spectrum of a light source or chromophores embedded inside a *weak* 3D photonic crystals that has stop bands but lacks a complete photonic band-gap. In such photonic crystals, the refraction index contrast between the constituent materials is not large enough to considerably alter the photon DOS. The PL spectra in weak 3D photonic crystal opals infiltrated with dye molecules or π-conjugated polymers were measured previously [49], where stop-bands in the emission spectra were clearly observed. In that work it was concluded that due to the weak influence of the underlying photonic crystal over the photonic DOS, then the modified PL spectrum was mainly induced by the transmission through the opal, rather than modification of the photon DOS. In our case too, the SPP excitations on the metal interfaces do not considerably alter the MIR photon DOS of the thermal radiating element, but mainly act as a

radiation filter [50] to the slightly modified emissivity spectrum.

It is worth noting, however that the ability of a *stronger* 3D photonic crystal to modify the absorption and thermal emission may indeed enhance the performance of lasers, detectors [51], solar cells, and infrared thermal image control [52]. These applications may therefore justify further investigations of non equilibrium thermal emission from meta-materials [53].

4. CONCLUSION

In conclusion, we measured the extraordinary optical transmission spectrum through a sub-wavelength hole array on an optically opaque Al film in the MIR spectral range. The transmission spectrum contains both resonances and anti-resonances optical features superposed on a smooth continuous band, and is well explained using the model of light coupling to SPP excitations on the two film interfaces. The effective dielectric response function of the hole array was calculated using a generalized form of a LST-type dielectric function that describes the resonant modes in the presence of an effective plasma frequency due to the individual holes. From the fitted dielectric response we calculated the absorption spectrum and found that it contains optical features that are opposite in phase to the resonant bands in transmission, in contrast to the obtained spectra in the visible spectral range.

The thermal emission spectrum measured from the hole array was found to have a close correspondence with the transmission spectrum, whereas the calculated absorption spectrum differed significantly. Further extraction of the effective 'transfer function' and a comparison with the transmission spectrum led us to conclude that such hole array structures behave as radiation filters by suppressing the emission outside their transmission bands. We thus conclude that plasmonic lattices cannot strongly modify the thermal emission spectrum, in contrast to what was expected previously.

ACKNOWLEDGEMENTS

We thank M. Delong for help with the FTIR measurements. This work was supported in part by the NSF grant # 08-01965.

REFERENCES

[1] H. Raether, *Surface Plasmons on Smooth and Rough Surfaces and on Gratings*, Springer-Verlag, Berlin, (1988).
[2] T. W. Ebbesen, H. J. Lezec, H. F. Gaemi, T. Thio, and P. A. Wolff, *Nature* (London) **391**, 667 (1998).
[3] H. F. Ghaemi, T, Thio, D. E. Grupp, T. W. Ebbesen, and H. J. Lezec, Phys. Rev. B **58**, 6779 (1998).
[4] T. J. Kim, T. Thio, T.W. Ebbesen, D. E. Grupp, and H. J. Lezec, Opt. Lett. **24,** 256 (1999).
[5] M. M. J. Treacy, App. Phys. Lett. **75,** 606 (1999).
[6] L. Martin-Moreno, F. J. Garcia-Vidal, H. J. Lezec, K. M. Pellerin, T. Thio, J. B. Pendry, and T. W. Ebbesen, Phys. Rev. Lett. **86,** 1114 (2001).
[7] A. Krishnan, T. Thio, T. J. Kim, H. J. Lezec, T. W. Ebbesen, P. A. Wolff, J. Pendry, L. Martin-Moreno, and F. J. Garcia-Vidal, Opt. Commun. **200,** 1 (2001).
[8] W. L. Barnes, A. Dereux, and T. W. Ebbesen, *Nature* (London) **424,** 824 (2003).
[9] J. G. Rivas, C. Schotsch, P. H. Bolivar, and H. Kurtz, Phys. Rev. B **68,** R201306 (2003).
[10] C. Schotsch, P. H. Bolivar, and H. Kurtz, Phys. Rev. B **68,** R201306 (2003).
[11] M. Sarrazin, J. P. Vigneron, and J. M. Vigoureux, Phys. Rev. B **67**, 085415 (2003).
[12] W.L. Barnes, W.A. Murray, J. Dintinger, E. Devaux, T.W. Ebbesen, Phys. Rev. Lett. **92**, 107401 (2004).
[13] K. J. K. Koerkamp, S. Enoch, F. B. Segerink, N. F. van Hulst, and L. Kuipers, Phys. Rev. Lett. **92**, 183901 (2004).
[14] H. J. Lezec and T. Thio, Opt. Express **12,** 3629 (2004).
[15] H. Cao and A. Nahata, Opt. Express **12,** 1004 (2004).
[16] Y. H. Ye and J. Y. Zhang, Appl. Phys. Lett. **84,** 2977 (2004).
[17] P. Lalanne, J.C. Rodier, and J.P. Hugonin, J. Opt. A: Pure Appl. Opt. **7,** 422 (2005).
[18] F. J. Garcia de Abajo, J. J. Saenz, I. Campillo, and J. S. Dolado, Opt. Express **14**, 7 (2006).
[19] A. Agrawal and A. Nahata, Opt. Express, 14, 1973 (2006).

[20] G. Gay, O. Alloschery, B. Viaris de Lesegno, C. O'Dwyer, J. Weiner, and H. J. Lezec, Nature Physics 2, 262 (2006).
[21] M. Sun, J. Tian, Z. Y. Li, B. -Y. Cheng, D. -Z. Zhang, A. Z. Jin, and H. F. Yang, Chin. Phys. Lett. **23**, 486 (2006).
[22] F. Przybilla, C. Genet, and T. W. Ebessen, Appl. Phys. Lett. **89**, 121115 (2006).
[23] T. Matsui, A. Agrawal, A. Nahata, and Z. V. Vardeny, *Nature* (London) **446,** 517 (2007).
[24] N. Papasimakis, V. A. Fedotov, F. J. Garcia de Abajo, A. S. Schwanecke, and N. I. Zheludev, arXiv:0704.2552v1, 19 Apr. 2007.
[25] J. Bravo-Abado, A. I. Fernandez,-Dominquez, F. J. Garcia-Vidal, and L. Martin-Moreno; preprint, June 13, 2007.
[26] Y. J. Bao, B. Zhang, Z. Wu, J. -W. Si, M. Wang, R. W. Peng, X. Lu, J. Shao, Z. F. Li, X. -P. Hao, and N. B. Ming, Appl. Phys. Lett. **90**, 251914 (2007).
[27] T. Neumann, M. L. Johanson, D. Kambhampati, and W. Knoll, Adv. Func. Mater. **12**, 575 (2002).
[28] P. A. Hobson, S. Wedge, J. A. E. Wasey, I. Sage, and W. L. Barnes, Adv. Mater. **14**, 1393 (2002).
[29] C. Liu, V. Kamaev, and Z. V. Vardeny, Appl. Phys. Lett. 86, 143501 (2005).
[30] R. Ziblat, V. Lirtsman, D. Davidov, and B. Aroeti, Biophys. Jour. **90**, 1 (2006).
[31] J. G. Fleming, S. Y. Lin, I. El-Kady, R. Biswas, K. M. Ho, *Nature* (London) **417,** 52 (2002).
[32] C. M. Cornelius and J. P. Dowling, Phys. Rev. A 59, 4736 (1999).
[33] S. Y. Lin, J. G. Fleming, E. Chow, J. Bur, K. K. Choi and A. Goldberg, Phys. Rev. B **62,** R2243 (2000).
[34] M. U. Pralle, N. Moelders, M. P. McNeal, I. Puscasu, A. C. Greenwald, J. T. Daly, E. A. Johnson, T. George, D. S. Choi, I. El-Kady, and R. Biswas, Appl. Phys. Lett. 81, 4685 (2002).
[35] S. Y. Lin, J. Moreno, and J. G. Fleming, Appl. Phys. Lett. **83,** 380 (2003).
[36] S. Y. Lin, J. G. Fleming, and I. El-Kady, Appl. Phys. Lett. **83**, 593 (2003); Yong-Sung Kim, Shawn-Yu Lin, Allan S. P. Chang, Jae-Hwang Lee and Kai-Ming Ho, J. Appl. Phys. **102** 063107 (2007).
[37] C. Lao, A. Narayanswamy, G. Chen, and J. D. Joannopoulos, Phys. Rev. Lett. **93,** 213905 (2004).
[38] S. Y. Lin, J. G. Fleming, and J. Moreno, Appl. Phys. Lett. **84,** 1999 (2004);
[39] I. El-Kady, W. W. Chow, and J. G. Fleming, Phys. Rev. **72,** 195110 (2005).
[40] T. Trupke, P. Wurfel, and M. A. Green, Appl. Phys. Lett. **84,** 1997 (2004); S. Y. Lin, J. Morebno, and J. G. Fleming, Appl. Phys. Lett. **84**, 1999 (2004).
[41] J. G. Fleming, Appl. Phys. Lett. **86,** 249902 (2005).
[42] I. Puscasu, M. Pralle, M. McNeal, J. Daly, A. Greenwald, E. Johnson, R. Biswas, and C. G. Ding, J. Appl. Phys. **98,** 13531 (2005).
[43] A. Agrawal, Z. V. Vardeny, and A. Nahata, Opt. Express **16**, 9601 (2008).
[44] R. H. Lyddane, R. G. Sachs and E. Teller, Phys. Rev. **59,** 673 (1941); E. L. Albuquerque, M. G. Cottam, *Polaritons in Periodic and Quasiperiodic Structures*, Elsevier B.V., Amsterdam, Chap. 1, 3 (2004).
[45] A. Mooradian, and G. B. Wright, Solid State Commun. **4,** 431 (1966).
[46] I. F. Chang and S. S. Mitra, Phys. Rev. **172,** 924 (1968).
[47] K. J. Nash, M. S. Skolnick, and S. J. Bass, Semicond. Sci. Technol. **2,** 329 (1987).
[48] E. M. Lifshitz, L. D. Landau, and L. P. Pitaevskii, *Electrodynamics of Continuous Media,* Academic Press, New York (1984).
[49] N. Eradat, M. Wohlgenannt, Z. V. Vardeny, A. A. Zakhidov, and R. H. Baughman, Synth. Metals **116,** 509 (2001).
[50] S. G. Romanov, T. Maka, C. M. Sotomayor Torres, M. Müller, and R. Zentel, Appl. Phys. Lett. **75**, 1057 (1999); E. P. Petrov, V. N. Bogomolov, I. I. Kalosha, and S. V. Gaponenko, Phys. Rev. Lett. **81,** 77 (1998).
[51] B. E. A. Saleh and M. C. Teich, *Fundamentals of Photonics,* John Wiley & Sons, New York, Chap. 17 pp. 648 (1991).
[52] F. K. Hopkins, Opt. Photonics News **9**, 32 (1998).
[53] S. John and R. Wang, Phys. Rev. B (submitted).

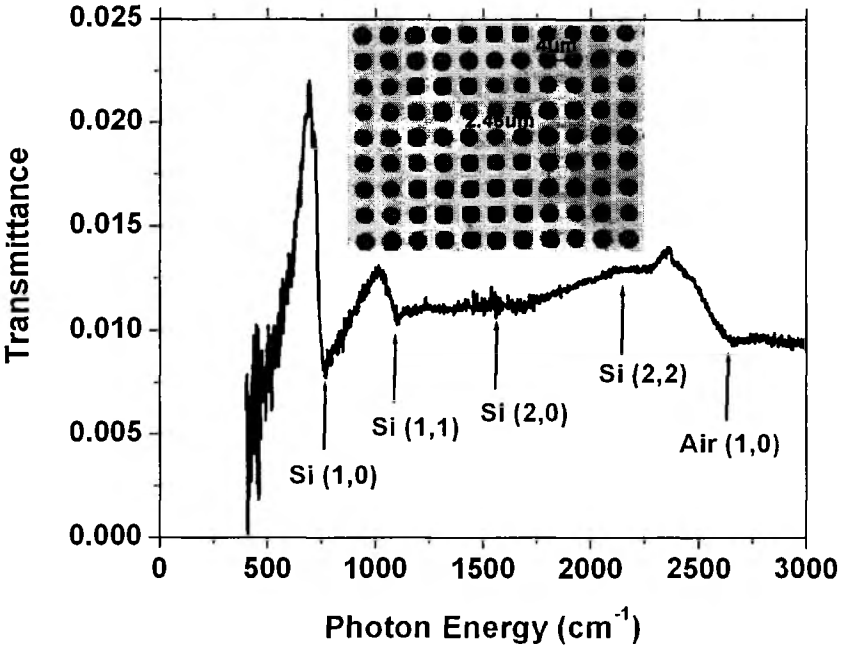

Figure 1 The optical transmission spectrum of an Al hole array (plasmonic lattice) at normal incidence. The arrows and labeled indices represent the surface plasmon modes associated with the different dielectric interfaces of the plasmonic lattice, namely, the substrate (Si) and air, respectively; the frequencies are given in Table I. The inset shows an optical microscope image of the plasmonic lattice sample, where the lattice constant $a = 4$ μm and aperture diameter $D = 2.46$ μm are assigned.

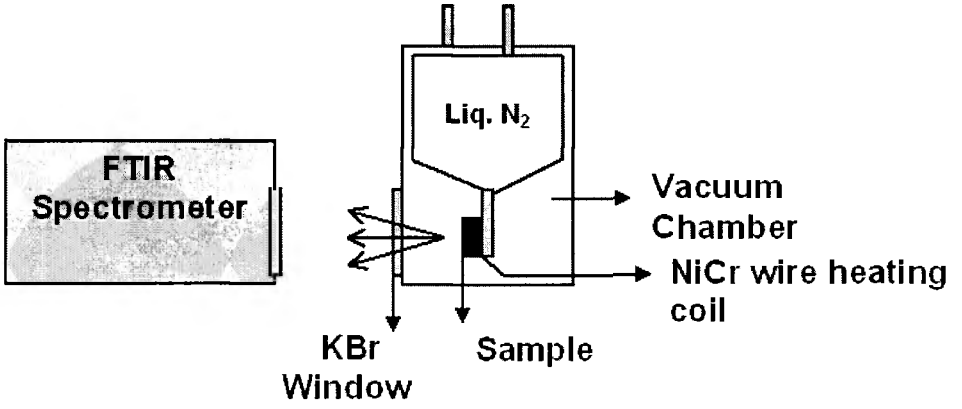

Figure 2 Schematic diagram of the thermal emission measurement setup. The sample is mounted on a NiCr wire heating coil and placed in a vacuum chamber supported by a long ceramic post that is connected to a liquid-nitrogen-cooled cold stage and heated to a temperature of about 600K during the measurement. The thermal emission spectrum is measured via an external port of a FTIR spectrometer.

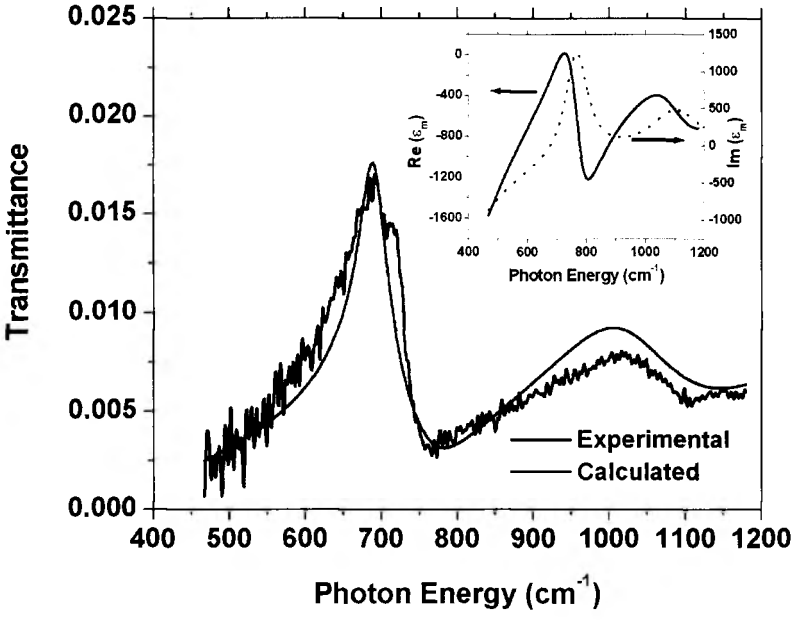

(a)

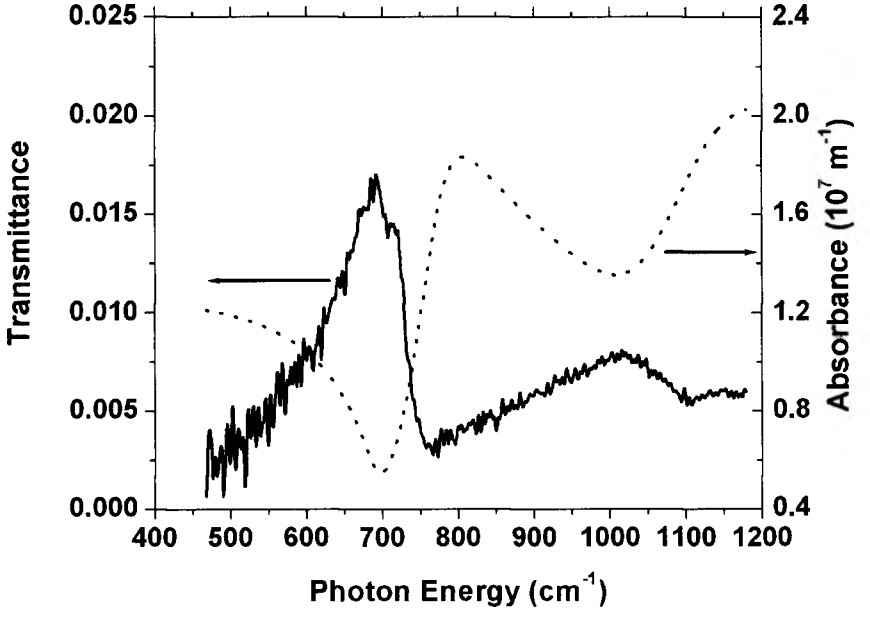

(b)

Figure 3 (a) A comparison between the experimental and calculated transmission spectra using $\varepsilon_m(\omega)$ calculated via Eq. 4 with the best fitting parameters given in Table II. The inset shows the corresponding calculated real and imaginary components of the dielectric response $\varepsilon_m(\omega)$. (b) The calculated absorption spectrum compared with the experimental transmission spectrum $T(\omega)$.

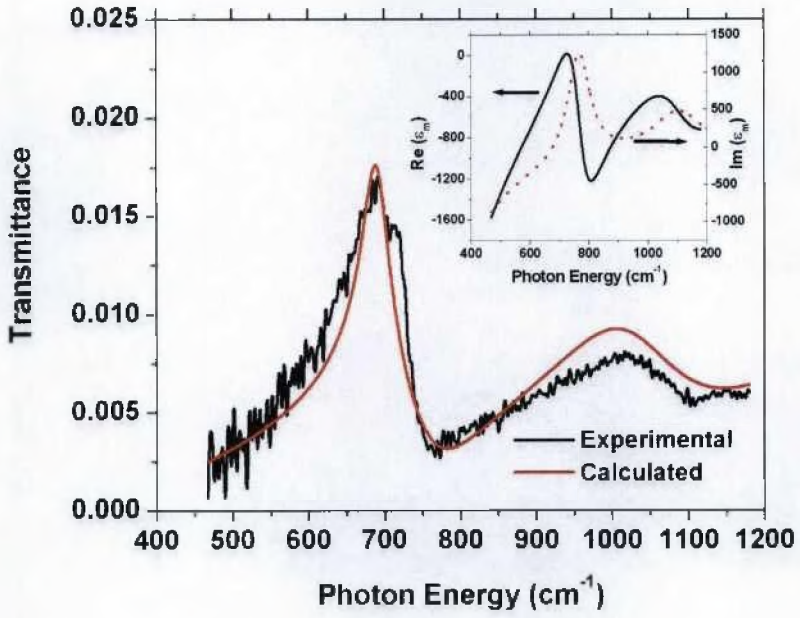

(a)

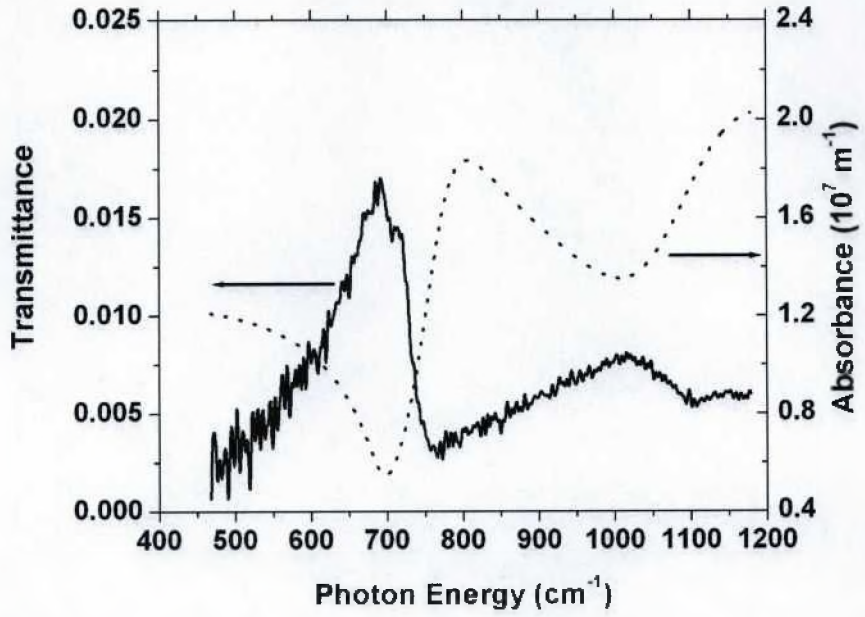

(b)

Figure 3 (a) A comparison between the experimental and calculated transmission spectra using $\varepsilon_m(\omega)$ calculated via Eq. 4 with the best fitting parameters given in Table II. The inset shows the corresponding calculated real and imaginary components of the dielectric response $\varepsilon_m(\omega)$. (b) The calculated absorption spectrum compared with the experimental transmission spectrum $T(\omega)$.

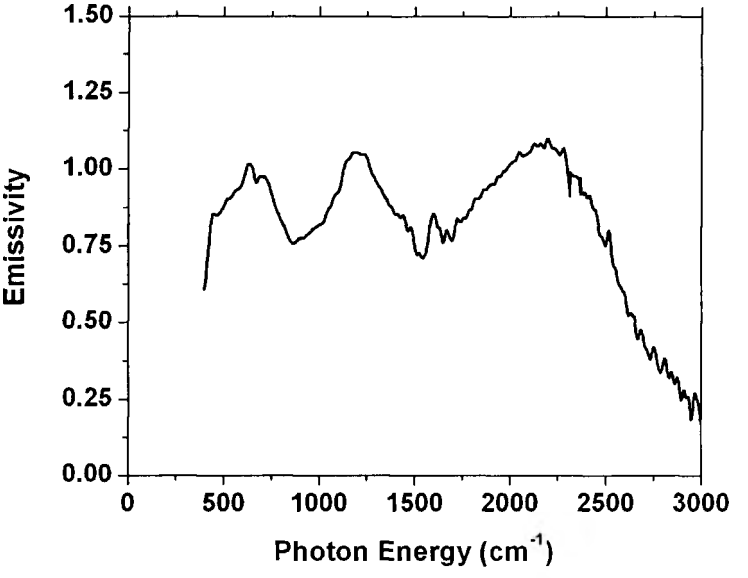

(a)

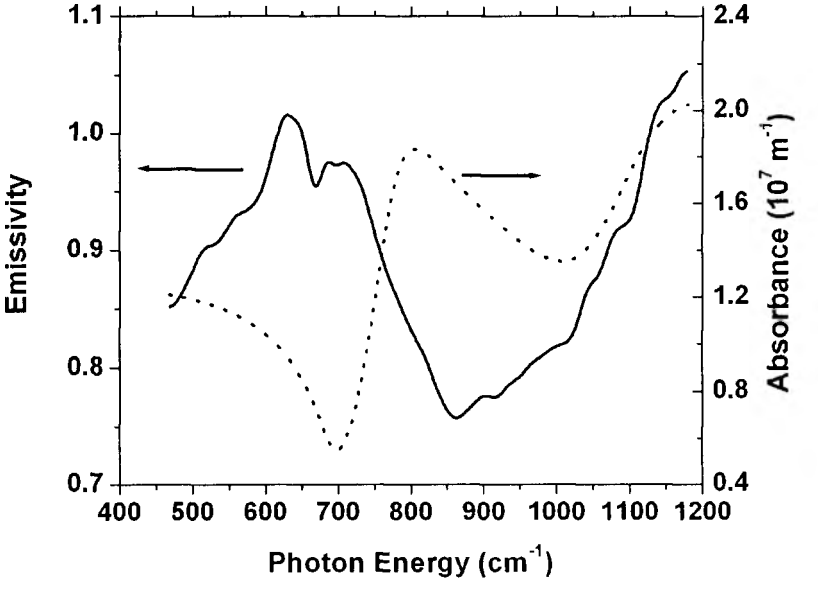

(b)

Figure 4 (a) The normalized emissivity spectrum $E(\omega)$ of the plasmonic lattice sample using the procedure described in Eq. 5. (b) Comparison between the $E(\omega)$ and $\alpha(\omega)$ spectra.

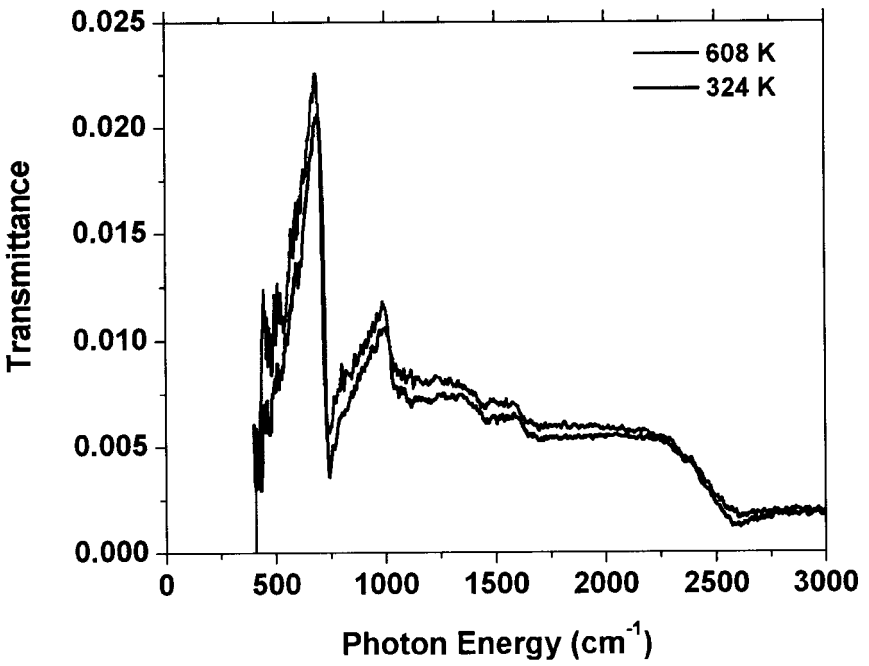

Figure 5 Transmission spectra of the Si-supported Al hole array measured at normal incidence at temperatures of 324 and 608 K.

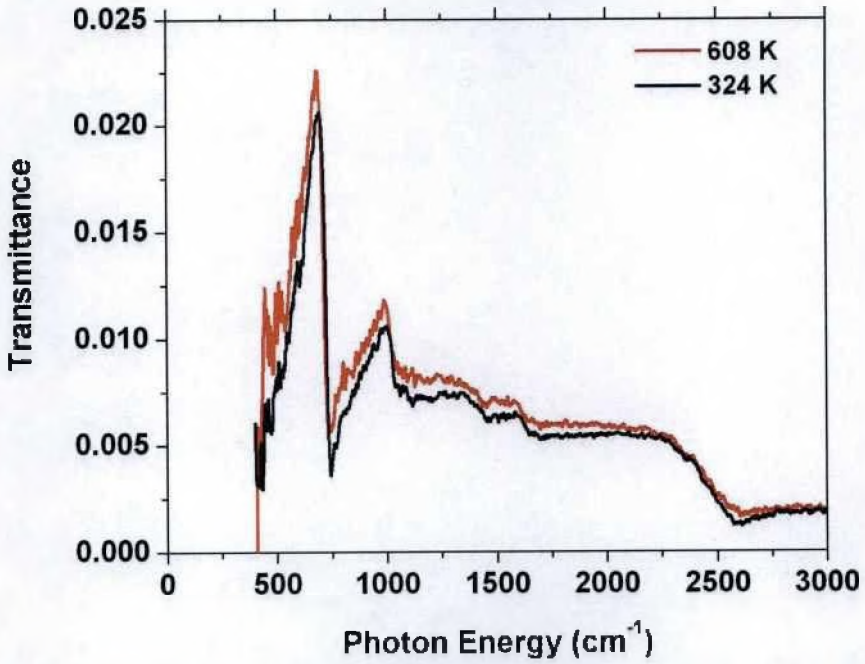

Figure 5 Transmission spectra of the Si-supported Al hole array measured at normal incidence at temperatures of 324 and 608 K.

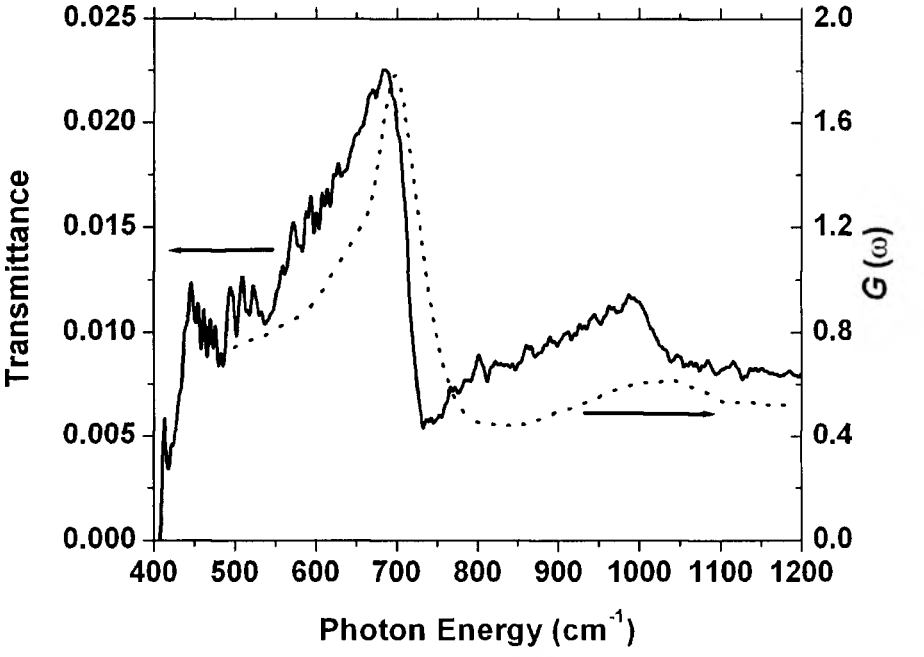

Figure 6 The transfer function $G(\omega)$ (dashed line, right scale) calculated from the emissivity and absorption spectra shown in Fig. 4(a) compared with the measured $T(\omega)$ spectrum at the same temperature of the thermal emission experiment (full line, left scale).